RUHR-UNIVERSITÄT BOCHUM
INSTITUT FÜR EXPERIMENTALPHYSIK V

Experimental Techniques in Plasma Spectroscopy

H.-J. Kunze

IAEA/ICTP Workshop on Plasma Physics,
Trieste, November 10 - 15, 2003

Wrong results by faulty experimental techniques

Effect of momentum transfer on the Rayleigh scattering cross section
Phys. Rev. A **19**, 2260 (1978)

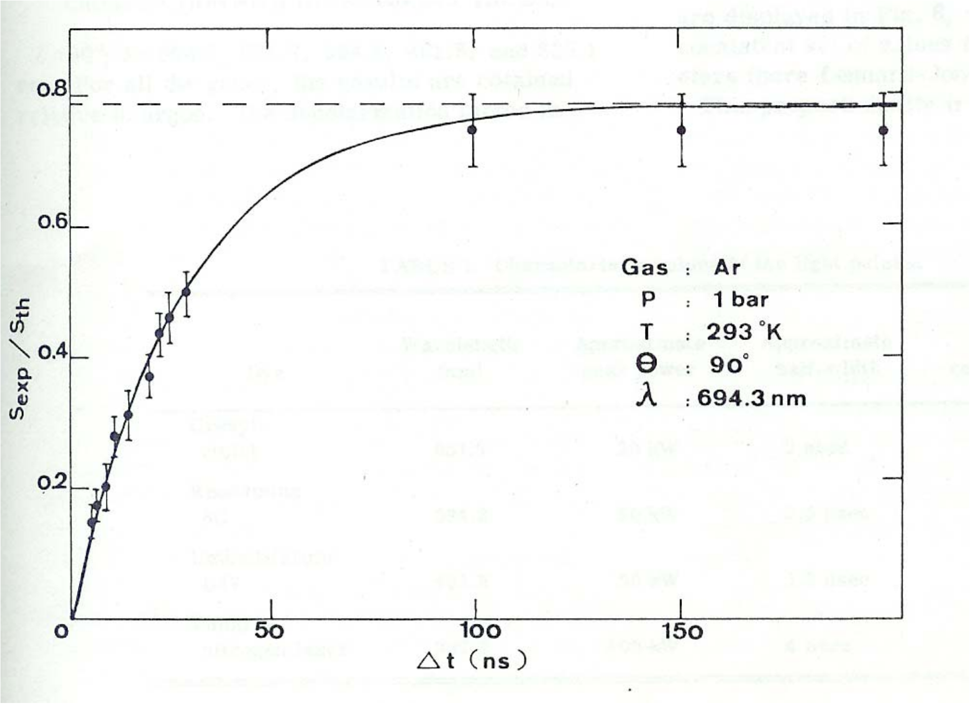

Cross section apparently became smaller with decreasing pulse duration of incident laser pulse

Puzzle remained for some time although other experiments (Phys. Lett. A57 (1978)) showed that the results must be wrong

What did they do wrong?

Signal from laser monitor and signal of scattered radiation were displayed on same oscilloscope with the scattered signal delayed by a long cable !

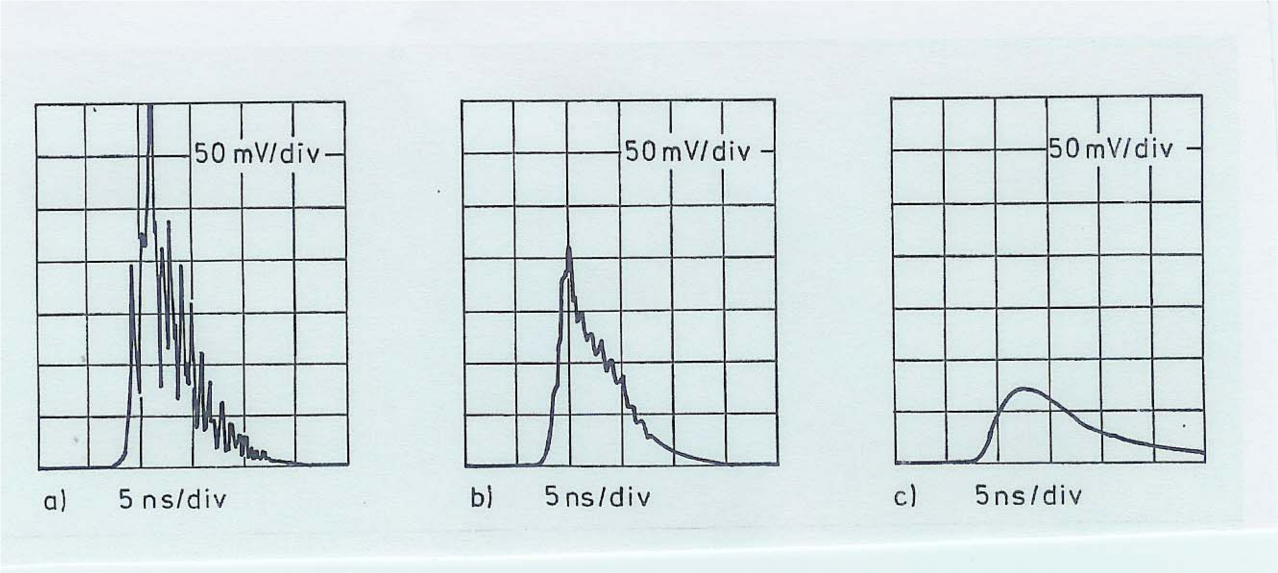

Signal from a photodiode recorded with a fast oscilloscope with a cable RG 58 C/U

a) 1 m long b) 11 m long c) 79 m long

Puzzle found a simple explanation

Extreme ultraviolet spectroscopy of helium-hydrogen plasma

R. Mills and P. Pay

J. Phys. D: Appl. Phys. **36**, 1535 (2003)

They report observation of novel emission lines

which they can explain only if they postulate

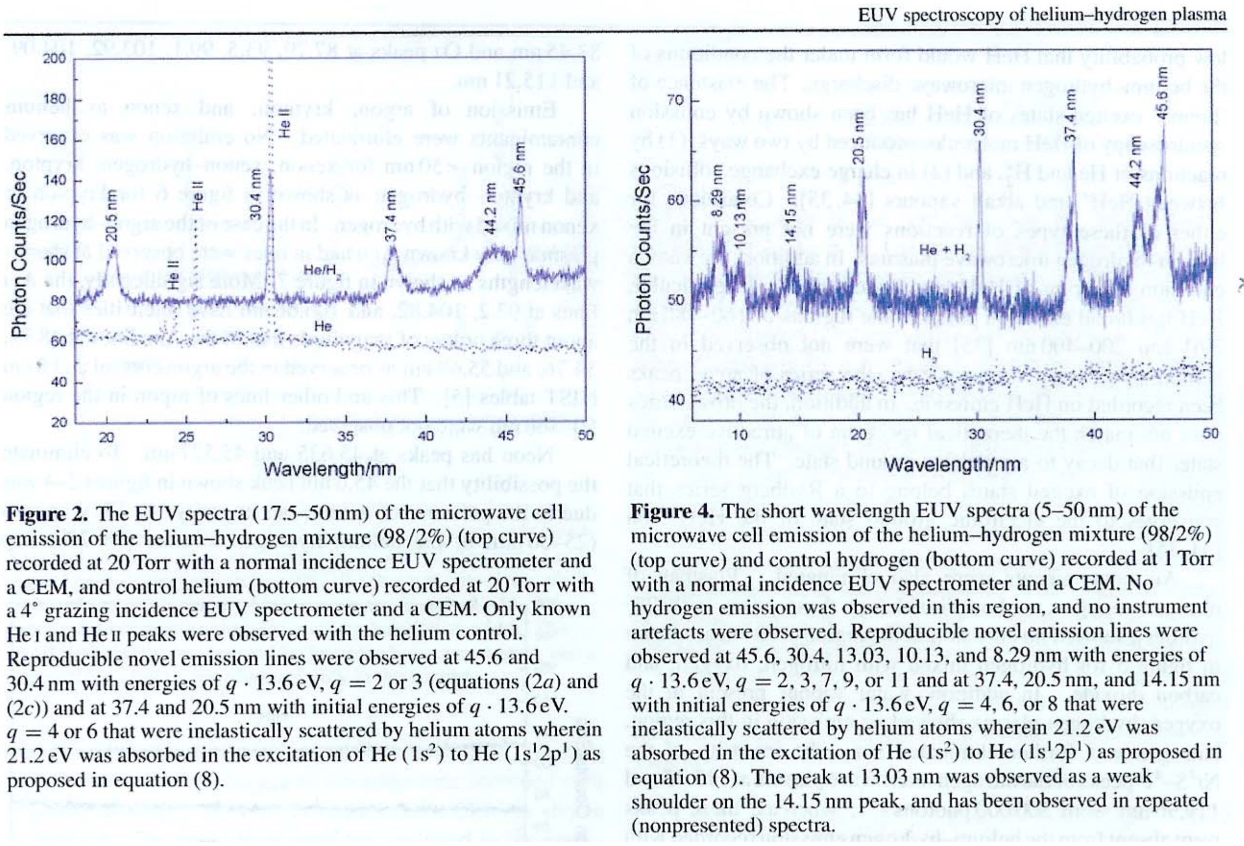

EUV spectroscopy of helium–hydrogen plasma

Figure 2. The EUV spectra (17.5–50 nm) of the microwave cell emission of the helium–hydrogen mixture (98/2%) (top curve) recorded at 20 Torr with a normal incidence EUV spectrometer and a CEM, and control helium (bottom curve) recorded at 20 Torr with a 4° grazing incidence EUV spectrometer and a CEM. Only known He I and He II peaks were observed with the helium control. Reproducible novel emission lines were observed at 45.6 and 30.4 nm with energies of $q \cdot 13.6$ eV, $q = 2$ or 3 (equations (2*a*) and (2*c*)) and at 37.4 and 20.5 nm with initial energies of $q \cdot 13.6$ eV, $q = 4$ or 6 that were inelastically scattered by helium atoms wherein 21.2 eV was absorbed in the excitation of He ($1s^2$) to He ($1s^1 2p^1$) as proposed in equation (8).

Figure 4. The short wavelength EUV spectra (5–50 nm) of the microwave cell emission of the helium–hydrogen mixture (98/2%) (top curve) and control hydrogen (bottom curve) recorded at 1 Torr with a normal incidence EUV spectrometer and a CEM. No hydrogen emission was observed in this region, and no instrument artefacts were observed. Reproducible novel emission lines were observed at 45.6, 30.4, 13.03, 10.13, and 8.29 nm with energies of $q \cdot 13.6$ eV, $q = 2, 3, 7, 9$, or 11 and at 37.4, 20.5 nm, and 14.15 nm with initial energies of $q \cdot 13.6$ eV, $q = 4, 6$, or 8 that were inelastically scattered by helium atoms wherein 21.2 eV was absorbed in the excitation of He ($1s^2$) to He ($1s^1 2p^1$) as proposed in equation (8). The peak at 13.03 nm was observed as a weak shoulder on the 14.15 nm peak, and has been observed in repeated (nonpresented) spectra.

quantum numbers n = 1/q for hydrogen,

where q is an integer. Novel physics ?

However, normal incidence spectrometers never work below about 30 nm, since mirrors and gratings do not reflect !!! Observation is an artifact !

Signal current from a photomultiplier is limited

Several saturation effects !

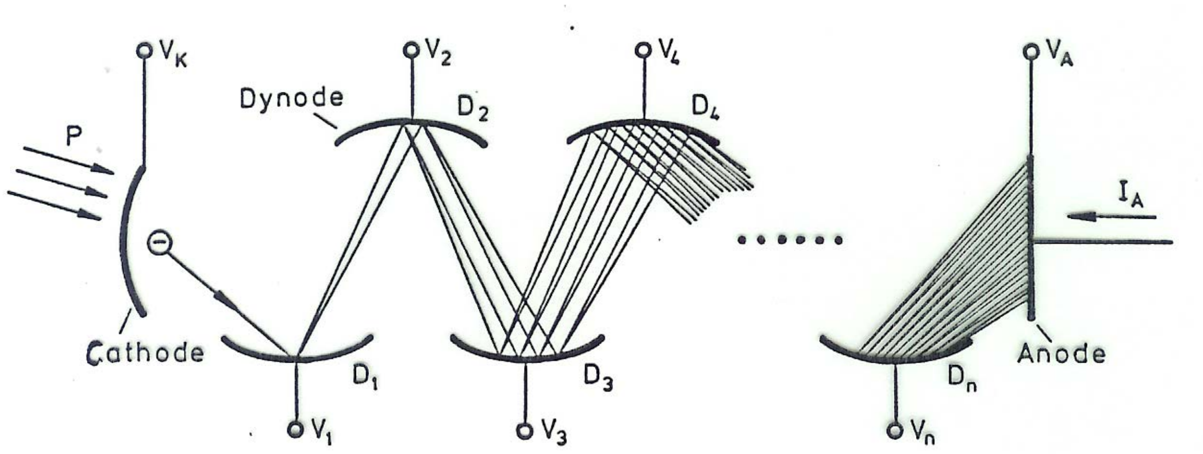

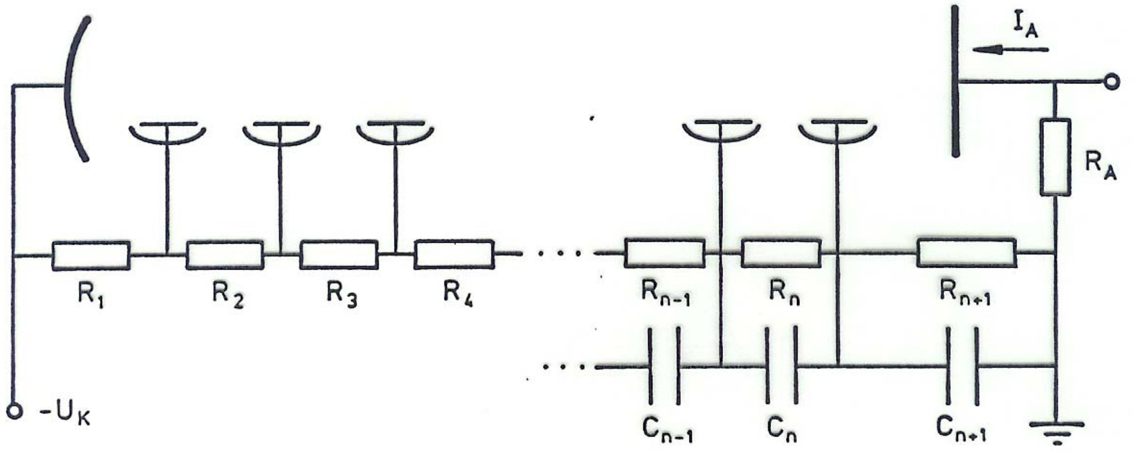

Capacitors parallel to the voltage divider must be dimensioned according to application

1 Introduction

Spectroscopic methods offer a large variety of possibilities to diagnose plasmas in the laboratory and in space, the apparatus required being one of the least complicated in many cases. Astronomical objects are the sun, the stars and the interstellar matter. Plasmas in the laboratory range at low temperatures from low density plasmas as nowadays mostly used for plasma processing to high density arcs and plasma torches at atmospheric pressure; at high temperatures pulsed but long-lived low density plasmas in magnetically confined fusion devices such as tokamaks and stellarators are at one end, short-lived inertially confined pellets having densities up to 10 000 times solid state density represent the other end.

Specifically we talk of plasma *emission* spectroscopy if electromagnetic radiation emitted by the plasma is recorded, spectrally resolved, analyzed and interpreted in terms of either parameters of the plasma or characteristic parameters of the radiating atoms, ions or molecules. It is the most straightforward approach since only one opening in closed systems is needed for radiation to emanate. The inherent drawback is certainly the fact that the radiation detected and hence all information obtainable is integrated along the line of sight. This also holds for the supplementary approach of *absorption* spectroscopy where radiation – in the most general case continuum radiation – is directed through the plasma and the modification of the spectrum of the transmitted radiation by absorption and also by scattering contains the information on the plasma and its constituents. The application of fixed wavelength and tunable lasers as radiation sources utilizing both absorption and various scattering processes in the plasma is widespread and has developed into a field of its own described as laser spectroscopy. It is no subject of this book and we refer to the relevant literature, for example to [1], or specifically with respect to the diagnostics of plasmas to [2]. Scattering by plasma electrons known as incoherent and collective Thomson scattering, one of the most powerful plasma diagnostic techniques [3], [4], [5], [6] is only mentioned here as well.

Most spectroscopic methods utilize the radiation emitted by atoms, ions or molecules being present in the specific plasma either as impurities or being intentionally added to the plasma for specific purposes such as radiation cooling or diagnostics. In recent years the injection of atomic beams has been advanced: they enter the plasma more or less on a straight path till they are ionized. As Fig. 1.1 reveals observation of the emission from the beam particles now yields *local* information from the hatched region, background radiation naturally still being collected along the line of sight.

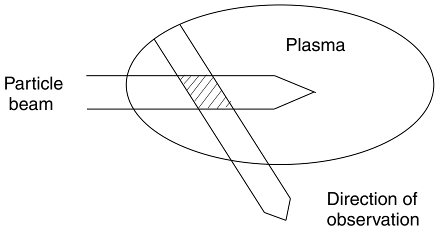

Fig. 1.1. Injection of a particle beam into a plasma

Spectral regions

With increasing temperature of a plasma the maximum of the continuum radiation and the strong lines emitted occur at shorter wavelengths, and typically plasma spectroscopy has to cover the spectral range from the infrared down to the x-rays. Although the physical concepts underlying the emission of radiation are more or less the same over this spectral range, different experimental techniques have to be employed resulting in a corresponding partition into several spectral ranges.

380–750 nm, the "visible". This spectral region is well defined by the sensitivity curve of the eye. Radiation is transmitted through air with practically no losses as it is for the adjacent regions towards shorter and longer wavelengths. The *"infra-red"* IR extends from the *"near infra-red"* to he *"far infra-red"* FIR adjacent to the microwave region which starts around wavelengths of 1 mm, but transmission through air can be influenced by absorption within molecular bands of water vapor, carbon dioxide and other molecular constituents or pollutants. In addition, absorption by windows has to be considered, which also holds when going to wavelengths below the visible. Flint glass, for example, starts to absorb already around 380 nm, and for shorter wavelengths windows of quartz are advised; ordinary quartz cuts off at around 210 nm, but best quartz is satisfactory down to just below 180 nm. The spectral range *200–380 nm* is known as the *"ultraviolet"* UV.

Below 200 nm electromagnetic radiation is absorbed by air, first by oxygen starting at around 195 nm and then by nitrogen at 145 nm, and transmission through air occurs again only below 0.15 nm, when 30% of the radiation starts to be is transmitted through 1 m of air at atmospheric pressure. To avoid this absorption in air, spectrographic system and path of the radiation from the plasma have to be evacuated. For that reason the spectral range *200–0.15 nm* has been named the *"vacuum-ultraviolet or vacuum-uv"* VUV. Traditionally, this range is subdivided according to the optics which has to be employed. *Vacuum-uv* is thus specifically used for the range *105–200 nm*, where transparent window materials (LiF cuts off at 105 nm) and hence also lens optics are existent.

The range 105–0.15 nm is customarily named *"extreme-ultraviolet"* EUV or XUV and it includes *the "soft x-rays"* from *30–0.15 nm.*

Below 0.15 nm the region of the *"hard x-rays"* starts where it is more practical to use the photon energy unit in keV instead of the wavelength. Hard x-rays overlap with the broad range of *"γ-rays"* from about *10 keV to 250 MeV*; γ-quanta are typically emitted by nuclei.

Spectroscopic units

The electromagnetic radiation flux from a surface element plotted as function of frequency ν or wavelength λ is known as *spectrum.* Both are related to each other by

$$\lambda_{vac} = c/\nu \tag{1.1}$$

where c and λ_{vac} are velocity of light and wavelength in vacuum, respectively, and ν is in Hertz ($1\,\mathrm{Hz} = 1\,\mathrm{s}^{-1}$). The most common wavelength units are the nanometer (nm), the Ångström ($1\,\text{Å} = 10^{-1}\,\mathrm{nm}$) and the micrometer ($\mu$m). The wavenumber σ defined by

$$\sigma = 1/\lambda_{vac} = \nu/c \tag{1.2}$$

is more commonly used at long wavelengths especially when dealing with molecular transitions. Its unit is the inverse meter, but in practice wavenumbers are usually expressed in inverse centimeters cm^{-1}. This unit has been named Kayser (K), $1\,\mathrm{K} = 1\,\mathrm{cm}^{-1}$.

At short wavelengths the photon energy $E = h\nu$ is preferred in the unit electron volt (eV). Wavelength in vacuum - we omit the subscript "vacuum" from hereon - and energy are thus related by

$$\frac{h\nu}{\mathrm{eV}}\,\frac{\lambda_{vac}}{\mathrm{nm}} = 1239.842\ . \tag{1.3}$$

Wavelengths of atoms and their ionization stages may be found in a number of reference publications as well in data banks: one easily accessible and extremely useful data bank is that of the National Institute of Standards and Technology NIST at Gaithersburg, USA [7]: the data have been critically evaluated and compiled, and energy levels, configurations and transition probabilities are given as well. Since the energy E of the levels is given in the unit cm^{-1} ($1\,\mathrm{eV} \Rightarrow 8065.541\,\mathrm{cm}^{-1}$), the wavenumber of a transition and thus its vacuum wavelength is simply obtained from the difference of the energies of upper E_u and lower level E_l: $\sigma = E_u - E_l = 1/\lambda$. It is common practice that wavelengths above 200 nm (λ_n) are quoted in dry air containing 0.03% CO_2 at 101 325 Pa at a temperature of 288.15 K. Both wavelengths are related to each other by

$$\lambda_n = \lambda/n\ . \tag{1.4}$$

n is the index of refraction of air at the above conditions and is given by [8]

$$n = 1 + 6\,432.8 \times 10^{-8} + \frac{2\,949\,810}{146 \times 10^8 - \sigma^2} + \frac{25\,540}{41 \times 10^8 - \sigma^2}\ , \tag{1.5}$$

where σ is the wavenumber in cm^{-1}.

For molecular spectra the monographs by Herzberg are still the main source [9], [10]. A molecular database HITRAN, for example, is continuously being developed at the Harvard-Smithsonian Center for Astrophysics in Cambridge, USA, and may be consulted via internet [11].

The present monograph intends to give an introduction to plasma spectroscopy, and the two books by Griem [12] and [13] remain the standard references for this field. For a general introduction to spectroscopic principles and techniques the monograph [14] may be consulted.

2 Quantities of Spectroscopy

2.1 Radiometric Quantities

The total energy emitted by a plasma as electromagnetic radiation per unit time is called its *radiative loss* and plays a crucial role in all power balance considerations. As physical quantity it is a *radiant flux* $\varPhi$ (through the surface of the plasma), and its unit is the watt W. It is also called *radiant power*. *Radiant flux density* ϕ refers to the flux per unit area $\phi = \mathrm{d}\varPhi/\mathrm{d}A$ with the unit $\mathrm{W/m^2}$, irrespectively of whether the radiation is emitted from an area, crosses an imaginary surface in space, or falls onto an area A. In this latter case it is customary to call this flux density at the surface *irradiance* E. The energy deposited per unit area during a given time is the *fluence* $H = \int E \mathrm{d}t$, with the unit $\mathrm{J/m^2}$.

The SI quantity *radiance* L is defined as the radiant flux per unit projected area per solid angle $\varOmega$ [15]. Figure 2.1 illustrates the geometry, where θ is the angle between the normal of the surface element $\mathrm{d}A$ and the direction of the radiation.

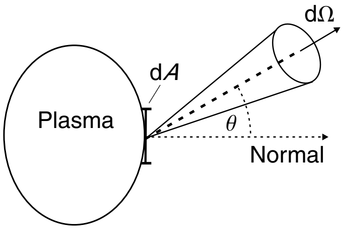

Fig. 2.1. Definition of radiance

$$L = \frac{\mathrm{d}^2\varPhi}{\mathrm{d}A\ cos\theta\ \mathrm{d}\varOmega} \tag{2.1}$$

Its unit is $\mathrm{W\,m^{-2}\,sr^{-1}}$. Again, it also applies to real and imaginary surfaces. Although the radiance is the correct SI unit, the rather familiar word *intensity* is still being used instead in much of the plasma spectroscopy literature. Confusion is unavoidable when authors use intensity for the radiation flux density. It is advisable, therefore, to check the unit whenever 'intensity' is encountered. The official SI quantity *radiant intensity* I is the flux per solid angle emitted from a source which makes it a property of a source rather than of a radiating surface: $I = \mathrm{d}\Phi/\mathrm{d}\Omega$, the unit being W/sr. In the field of physical optics the word 'intensity' refers to the magnitude of the Poynting vector.

For completeness the *radiant energy density* u (unit J/m^3) should be mentioned, which is usually employed in atomic and thermodynamic considerations. In case of isotropic radiation, for example, it is given by relation (a), and for collimated radiation in the other limit by relation (b):

$$(a) \quad u = \frac{4\pi}{c}\, L \qquad (b) \quad u = \frac{1}{c}\, L \tag{2.2}$$

The *local* emission at the position $\boldsymbol{r}$ in the plasma is characterized by the *emission coefficient* $\epsilon(\boldsymbol{r})$:

$$\epsilon(\boldsymbol{r}) = \frac{\mathrm{d}^2\Phi(\boldsymbol{r})}{\mathrm{d}V\,\mathrm{d}\Omega}\,, \tag{2.3}$$

where $\mathrm{d}\Phi(\boldsymbol{r})$ is the radiant flux from the volume element $\mathrm{d}V$ at $\boldsymbol{r}$. This assumes that the emission is isotropic. It can be, of course, also non-isotropic, when a specific direction is given by electric or magnetic fields or by fast particle beams. The unit of the emission coefficient is $\mathrm{W\,m^{-3}\,sr^{-1}}$.

With the exception of bolometric measurements usually spectral quantities are measured and they are denoted by the pertinent subscript λ (or ν or ω). They are derivative quantities and yield the total quantity when integrated over wavelength or frequency. For example $\epsilon(\boldsymbol{r}) = \int \epsilon_\lambda(\boldsymbol{r}, \lambda)\mathrm{d}\lambda$.

2.2 Measured Quantities

In the most straightforward case adiation from a plasma (for simplicity we take a plane surface with surface element $\mathrm{d}A_p$) falls on a detector with surface element $\mathrm{d}A_d$ positioned at a distance s, see Fig. 2.2: The quantity thus

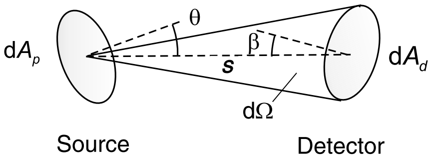

Fig. 2.2. Measured radiation

recorded is a flux Φ given according to (2.1) by

$$\Phi = \int L\, cos\theta\, \mathrm{d}A_p\, \mathrm{d}\Omega = \int L\, cos\theta\, \mathrm{d}A_p\, \frac{cos\beta\, \mathrm{d}A_d}{s^2}\,. \tag{2.4}$$

For small angles Φ reduces to

$$\Phi = L\ A_p\ \Omega_d = L\ \frac{A_p\ A_d}{s^2}\ . \tag{2.5}$$

Ω_d is the solid angle subtended by the detector area A_d.

For spectrally resolved measurements the radiation flux is limited by the area A_s of the entrance slit of a spectrographic instrument and by the size of a mirror, a lens, a dispersive element or a real or virtual aperture (cross section A_m). Figure 2.3 illustrates this geometry and it is obvious that the cross section A_m determines the area A_p of the source surface from which radiation is collected through the slit. Neglecting the transition at the boundary

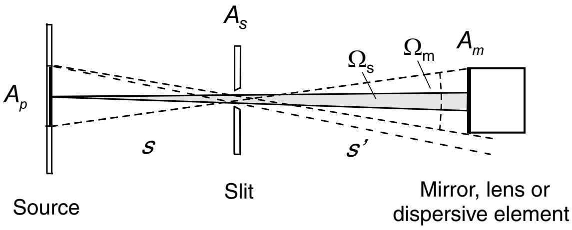

Fig. 2.3. Measured radiation

$$\Phi = L\ A_p\ \Omega_s = L\ A_p \frac{A_s}{s^2} = L\ A_s\ \frac{A_m}{s'^2} = L\ A_s \Omega_m\ . \tag{2.6}$$

The quantity $A_s\Omega_m$ is called the *throughput* or *étendue* of the instrument (it is conserved as we will see below), and the flux Φ is simply obtained as if the emitting surface were in the plane of the entrance slit.

This is readily exploited in quantitative measurements: a standard radiator of known radiance L_0 is placed close to the entrance slit, or in principle at any distance where its size is still sufficient to fill the solid angle Ω_m . The flux $\Phi_\lambda(\lambda)\Delta\lambda{=}L_{0\lambda}(\lambda)\Delta\lambda\ A_s\Omega_m$ over a spectral interval $\Delta\lambda$ will produce a signal S_0 at the exit of a detector. Keeping all settings constant the respective flux in the same spectral interval from an unknown radiator may give the signal S_x, hence

$$L_{x\lambda}(\lambda) = \frac{S_x}{S_0}\ L_{0\lambda}(\lambda)\ . \tag{2.7}$$

This is an extremely simple relation: the ratio of the signals yields the unknown spectral radiance $L_{x\lambda}(\lambda)$, and it is this quantity which is obtained in the measurement.

A plasma, on the other hand, emits throughout its volume, but the above considerations may also be applied directly if we replace the radiating surface of Fig. 2.3 by a slice of plasma of thickness ds. $A_p(s)$ just has to be smaller than the cross section of the plasma at the distance s. With no absorption within the plasma (2.3) and (2.6) yield

$$\varPhi = \int \epsilon(s)\,\mathrm{d}A_p(s)\,\mathrm{d}s\,\mathrm{d}\varOmega = \left(\int \epsilon(s)\mathrm{d}s\right)\, A_p\varOmega_s \;= L\,A_s\varOmega_m \tag{2.8}$$

$$\text{with} \qquad L = \int \epsilon(s)\mathrm{d}s \tag{2.9}$$

L is the radiance at the surface of the plasma and will also be again the effective radiance in the plane of the entrance slit.

For a correctly designed optical system, reduced to a lens of diameter D in Fig. 2.4, we have for object and image size y and y' with object and image distance s and s', respectively,

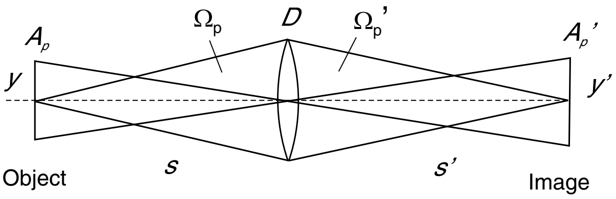

Fig. 2.4. Imaging by a lens

$$\frac{y/2}{y'/2} = \frac{s}{s'}\ , \tag{2.10}$$

and hence

$$\frac{y^2}{s^2}\,D^2 = \frac{y'^2}{s'^2}\,D^2 \qquad \Longrightarrow \qquad A_p\varOmega_p = A_p{}'\varOmega_p{}'\ . \tag{2.11}$$

The throughput is conserved. Since also the radiant flux $\varPhi$ remains constant, (2.8) and (2.11) yield directly the well known law

$$L = L' \tag{2.12}$$

i.e. the radiance is an invariant of an optical system with no absorption.

In case the cross section of the plasma is smaller than the area A_p at the position s (Fig. 2.3), the full throughput is not utilized. In this case the plasma should be imaged onto the entrance slit employing a lens or a spherical mirror. These considerations also apply when a large plasma is to be investigated spatially resolved. Figure 2.5 illustrates such an arrangement. The lens produces a virtual image (area A_s') of the entrance slit, and only radiation from the shaded region is collected by the lens and the virtual slit

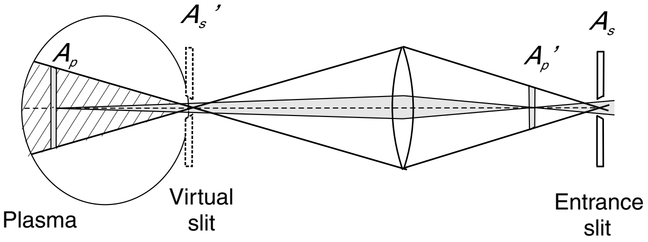

Fig. 2.5. Spatially resolved measurements

and hence also by the entrance slit. This geometry corresponds exactly to that of Fig. 2.3 with a radiance $L = \int \epsilon \mathrm{d}s$ at the position of the virtual slit and according to (2.12) also at the entrance slit: the quantity obtained is the *local* radiance at the surface of the plasma, given by the integral of the emission coefficient ϵ along the line of sight. One certainly has to select a lens of sufficient diameter, that the full throughput is used in the spectrographic instrument.

2.3 Local Quantities

2.3.1 Homogenous Plasmas

The discussions in the preceding sections showed that the quantity measured is always the local radiance at the surface of the plasma which is given by integration of the emission coefficient along the line of sight when no absorption of radiation within the plasma is important. Hence only an average emission $\overline{\epsilon}$ can be quoted,

$$\overline{\epsilon} = \frac{L}{s_2 - s_1} , \tag{2.13}$$

where $s_2 - s_1$ is the depth of the plasma along the line of sight. For a homogeneous plasma this corresponds to the true emission coefficient ϵ.

2.3.2 Axially and Spherically Symmetric Plasmas

In cases of axially symmetric plasma columns the derivation of local emission coefficients $\epsilon(r)$ is possible if the radiance of the plasma is measured over the cross section of the column. Integration along a chord parallel to the x-axis yields after substituting $x^2 = r^2 - y^2$ (Fig. 2.6) the one-dimensional profile of the radiance

$$L(y) = 2 \int_0^{x_{max}} \epsilon(r) \, \mathrm{d}x = 2 \int_0^{\sqrt{R^2 - y^2}} \epsilon(r) \, \mathrm{d}x = 2 \int_y^R \frac{\epsilon(r) \, r \, \mathrm{d}r}{\sqrt{R^2 - y^2}} . \tag{2.14}$$

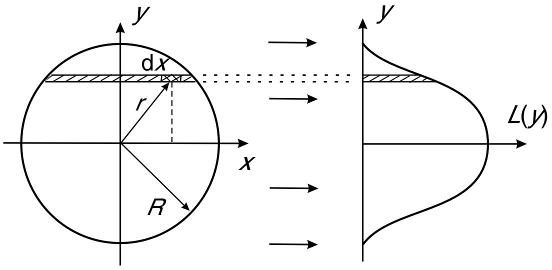

Fig. 2.6. Radiance parallel to the y-axis of a cylindrically symmetric plasma column

This equation is of the Abel type, and the local emission coefficient $\epsilon(r)$ is recovered by the Abel inversion which can be written analytically as

$$\epsilon(r) = -\frac{1}{\pi}\int_r^R \frac{\mathrm{d}L(y)}{\mathrm{d}y}\frac{\mathrm{d}y}{\sqrt{y^2 - r^2}}\,. \tag{2.15}$$

Since the spatial derivative $\mathrm{d}L/\mathrm{d}y$ enters the inversion, it is obvious that the results are very sensitive to noise and errors in the measured radiance $L(y)$. Unfortunately the errors in the derivative accumulate over the integration interval $[r,R]$, and the resulting uncertainty is most severe on the axis $r = 0$. Hence appropriate smoothing of the data can be essential for the quality of the inversion. An inversion algorithm without differentiation has been has been proposed by [16], and other improved inversion methods are mentioned in [13]. In cases of strongly structured emission profiles the finite solid angle of the radiation collecting optics has to be taken into account [17].

For spherically symmetric plasmas two-dimensional imaging forms an array $L(y, z)$ of the radiance in the y-z plane. Because of the symmetry it usually suffices to analyze the radiance $L(y, 0)$ in one plane ($z = 0$) to which the above cylindrical solution can be applied. Physically it corresponds to one-dimensional imaging employing a narrow slit in front of the plasma.

In the x-ray region the pinhole camera is the standard imaging system. It is simple, and the typically arrangement is shown in Fig. 2.7. Integration of the emission coefficient $\epsilon(r)$ is now along differing tilted chords. The

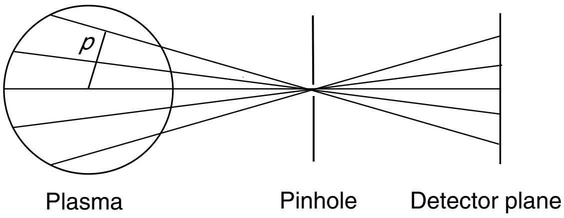

Fig. 2.7. Schematic arrangement of a pinhole camera

chordal heights p, or impact parameters, are calculated from the known geometric dimensions of the system, and the recorded radiances can then readily be transformed to the respective radiance distribution of parallel recording needed for the standard Abel inversion.

2.3.3 Plasmas Without Symmetry

One special case of non-axisymmetry exists in tokamaks which employ a limiter and have a circular poloidal cross-section: the magnetic flux surfaces and hence the density contour lines are very close to a set of nested eccentric circles, the shift of the circle centers being known as the Shafranov $\varDelta$ shift. With the transformation $r^2 = (x + \varDelta)^2 + y^2$ Abel inversion as discussed in the previous section can be again executed, and specific methods have been developed too [18], [19], [20]. In [21] the technique was extended to plasmas of elliptic shape which is transformed mathematically to a concentric circular shape for the analysis.

The mathematical problems associated with the general reconstruction of the local emission $\epsilon(\boldsymbol{r})$ throughout the plasma are essentially identical to those encountered in computer-aided tomography, drawing upon the same mathematical techniques [22]. The radiance of the plasma has to be recorded in numerous directions, and the Radon transformation and its inverse then provides the mathematical basis for the reconstruction. We shall consider here only the two-dimensional Radon transform, the extension to three dimensions is straightforward. Figure 2.8 illustrates the geometry and the definition of the coordinates. Integration is along straight lines given by ($\boldsymbol{n} = \{\cos\phi, sin\phi\}$ is a unit vector perpendicular to these lines)

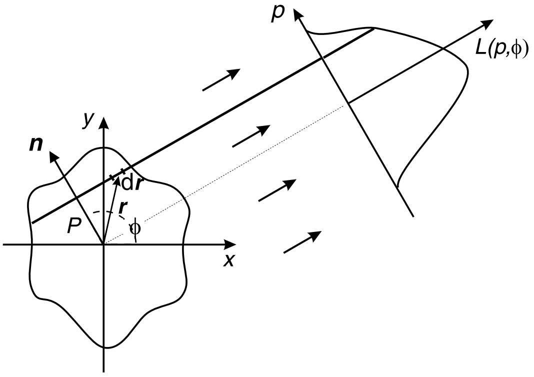

Fig. 2.8. Coordinate system for the Radon transform

$$\boldsymbol{r}\boldsymbol{n} - p = x\,\cos\phi + y\,\sin\phi - p = 0 \tag{2.16}$$

yielding the radiance

$$L(p,\phi) = \int_{-\infty}^{\infty}\int_{-\infty}^{\infty} \epsilon(x,y)\,\delta(x\cos\phi + y\sin\phi - p)\,\mathrm{d}x\mathrm{d}y \tag{2.17}$$

where $\delta(.)$ is the Dirac delta function. Because of the symmetry $L(p,\phi) = L(-p,\phi+\pi)$ only angles 0 to π are needed. Mathematically $L(p,\phi)$ is the Radon transform of $\epsilon(x,y)$

$$L(p,\phi) = \mathcal{R}_2\{\epsilon(x,y)\}\,. \tag{2.18}$$

For the execution of the inverse Radon transformation to obtain the emission $\epsilon(x,y)$ within the plasma,

$$\epsilon(x,y) = \mathcal{R}_2^{-1}\{L(p,\phi)\}\,, \tag{2.19}$$

a number of algorithms and numerous techniques are available, for example see [23]. The quality of the obtained reconstruction certainly depends on the number of views of the plasma, or precisely on the number of $L(p,\phi)$ values. Unfortunately these are usually limited due to experimental constraints as for example by the plasma vessel and its ports. The reconstruction is facilitated and improved if information on the plasma shape or its overall structure is available and can be utilized.

References

1. W. Demtröder: *Laser Spectroscopy*, 3rd edn (Springer, Berlin Heidelberg New York 2003)
2. K. Muraoka, M. Maeda: *Laser Aided Diagnostics of Plasmas and Gases*, (Institute of Physics Publishing, Bristol 2001)
3. H.-J. Kunze: The Laser as a Tool for Plasma Diagnostics. In: *Plasma Diagnostics*, ed by W. Lochte-Holtgreven (North-Holland, Amsterdam 1968) pp 550–616
4. A.W. DeSilva, G.C. Goldenbaum: Plasma Diagnostics by Light Scattering. In: *Methods of Experimental Physics* vol 9, ed by H.R. Griem, R.H. Lovberg (Academic Press, New York London 1970) pp 61–113
5. J. Sheffield: *Plasma Scattering of Electromagnetic Radiation*, (Academic Press, New York 1975)
6. S.H. Glenzer, W.E. Alley, K.G. Estabrook, et al: Phys. Plasmas **6**, 2117 (1999)
7. http://www.physics.nist.gov/PhysRefData/contents-atomic.html
8. C. Cowley, W.L. Wiese, J. Fuhr, and L.A. Kuznetsova: Spectra. In: *Allen's Astrophysical Quantities* fourth edition, ed by A. N. Cox (Springer, New York Berlin Heidelberg 1999) pp 55–93
9. G. Herzberg: *Spectra of Diatomic Molecules*, (Van Nostrand, New York 1959)
10. G. Herzberg: *Electronic Spectra of Polyatomic Molecules*, (Van Nostrand, New York 1966)
11. http://www.hitran.com
12. H.R. Griem: *Plasma Spectroscopy*, (McGraw-Hill, New York San Francisco Toronto London 1964)
13. H.R. Griem: *Priniples of Plasma Spectroscopy*, (Cambridge University Press, Cambridge 1997)
14. A. Thorne, U. Litzén, S. Johannson: *Spectrophysics-Principles and Applications*, (Springer, Berlin Heidelberg New York 1999)
15. *Le Système International d'Unités, The International Systems of Units*, (Bur. Intl. Poids et Mesures, Sèvres France 1998)
16. Yu.E. Voskoboinikov, N.G. Preobrazhenskii: Opt. Spectrosc. (USSR) **60**, 111 (1999)
17. K.T. Walsh, J. Fielding, M.B. Long: Opt. Lett. **25**, 457 (2000)
18. N. Gottardi: J. Appl. Phys. **50**, 2647 (1979)
19. H. Soltwisch: Rev. Sci. Instrum. **57**, 1939 (1986)
20. H.K. Park: Plasma Phys. Contr. Fusion **31**, 2035 (1989)
21. Y. Nagayama and A.W. Edwards: Rev. Sci. Instrum. **63**, 4757 (1992)
22. A.M. Cormack: J. Appl. Phys. **34**, 2722 (1963)
23. F. Natterer, F. Wuebbeling: *Mathematical Methods in Image Reconstruction*, (SIAM, Philadelphia 2001)

From: ASTROPHYSICAL & LABORATORY SPECTROSCOPY
Edited by R. Brown and J. Lang
(33. Scottish Universities Summer School in
Physics, 1988)

SPECTROMETER DESIGN AND LABORATORY APPLICATION

H.-J. Kunze

Ruhr-Universität, Bochum, Germany

1.

INTRODUCTION

The dream of a spectroscopist is a system that records the complete spectrum of electromagnetic radiation emitted by a plasma having, in addition, a spectral resolution in specified wavelength intervals that allows the analysis of line profiles. To top this, the spectrum should be recorded as a function of time at a rate determined by the rate of change of the emission. In comparison to such a system, the actual possibilities look rather lean. Nevertheless, if one restricts oneself to specific spectroscopic aspects, the requirements usually can be met. One critical component of any system is the detector. That subject will be discussed by I. Martinson.

The transmission properties of the electromagnetic radiation through air divide the spectrum quite naturally into three regions. Below about 200 nm, air absorbs the radiation, and the solution to this problem is to evacuate the complete spectrographic system. For this reason, this spectral region is called the *vacuum ultraviolet*. Helium, on the other hand, is transparent to radiation down to 53 nm, and air could simply be substituted by helium if the specific experimental conditions permit. Above 200 nm we have the ultraviolet and visible region. At short wavelengths, the vacuum uv overlaps the soft x-ray region. Below 0.15 nm, air starts transmitting again: at atmospheric pressure, the intensity transmitted through a layer 1 m thick is 30 % of the incident one. Substituting air by helium is advantageous also in this spectral region and may save the experimenter an expensive vacuum system: the transmission through a 1 m layer is 99% at 0.15 nm, and still 60% at 1 nm.

The windows, which may be necessary to separate the plasma containing chamber from the spectrometer, pose another problem. The most commonly used window in the vacuum uv is lithium fluoride (LiF). It has the shortest wavelength transmission limit of any material known, however, it loses its transmission gradually because of radiation damage. The onset of the transmission of the best fused quartz (suprasil) is at about 160 nm. On the lower end of the spectrum, metallic or organic films or foils are typically used as windows or filters. At 5 nm, for example, beryllium 100 μm thick transmits about 50%.

2.
SPECTROMETERS FOR THE VISIBLE AND ULTRAVIOLET

2.1 General considerations

A typical spectrometer consists of an entrance slit S_1 in the focal plane of a collimating spherical mirror M_1, a grating G as dispersing element, and a focussing mirror M_2 which forms an image of the entrance slit in the focal plane F (see Fig. 1). Due to the grating, the position of the image is a function $x(\lambda)$ of the wavelength. When used as *spectrograph*, a photographic plate or film is placed in this image plane and, depending on the dispersion and specific design of the instrument, a small or large spectral range can be recorded. The spectrum obtained is time-integrated. However, a fast mechanical shutter may be used at the entrance slit or a streak camera in the focal plane when recording the image. Modern developments of optical multichannel analyzers have brought about great changes. They allow the real-time observation of slowly changing spectra as well as, by gating the detector, the recording of a spectrum for time intervals down to the

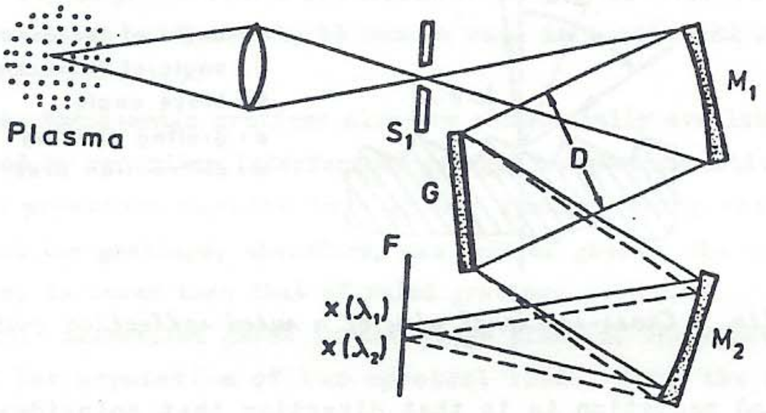

Fig. 1 Schematic of a spectrometer system

nanosecond range. When used as *monochromator*, an exit slit is placed in the image plane, and a photoelectric detector records nearly monochromatic radiation passing through this slit. Rotation of the grating by a gear box changes continuously the wavelength of the transmitted radiation and the photoelectric current thus represents directly a scan of the spectral emission of a stationary source. On the other hand, keeping the grating stationary, the detector records the temporal evolution of the spectral emission within the small spectral range selected by the width of the exit slit. A *polychromator* is a design with several exit slits and individual detectors. In many cases systems of optical fibers are used.

It is customary to use the name *spectrometer* for both the spectrograph and the monochromator version.

2.2 Some basic properties

In most spectrometers a grating is the dispersive element. Figure 2 shows a cross-sectional view of a *ruled* reflection grating. By ruling the grooves with flat faces and controlling the face angles θ of the grooves it is possible to concentrate the spectral energy in any desired angular region. This is called *blazing* a grating and the groove face angle is called *blaze angle*. The maximum intensity of the

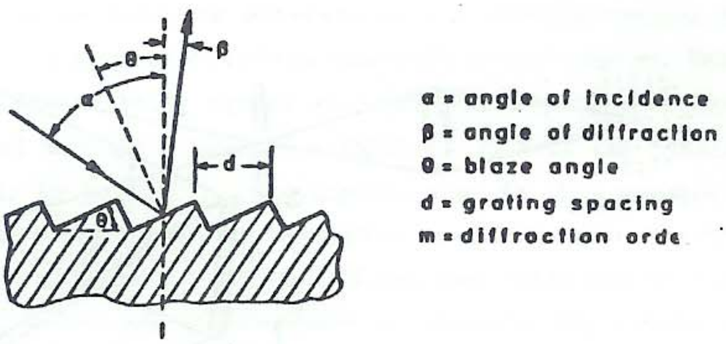

Fig. 2 Cross-sectional view of a ruled reflection grating

diffracted radiation is in that direction that coincides with the direction of the specularly reflected beam from the surface of the facet:

$$\alpha - \theta = \theta + \beta \tag{1}$$

The basic grating equation is

$$m\lambda = d\,(\sin\alpha - \sin\beta) \tag{2}$$

if angle of incidence α and angle of diffraction β are on different sides of the grating normal as shown in the figure. The wavelength λ_B corresponding to the strongest diffracted radiation then is given by

$$m\lambda_B = 2d\,\sin\theta\,\cos(\alpha - \theta) \tag{3}$$

Once a specific application has been identified, the blaze angle θ of the grating has to be selected accordingly. Grating manufacturers usually specify blaze angle and a first-order blaze wavelength λ_{B1} for normal incidence ($\alpha = 0$; $m = 1$), i.e. $\lambda_{B1} = d \sin 2\theta$. It is obvious from Eq. (3) that a grating blazed for λ_B in first order is also blazed for λ_B/m in the m-th order. The efficiency of such gratings (where the efficiency at a given wavelength is defined as the percentage of the incident flux returned by the grating into a given spectral order) may reach 90% at the blaze wavelength and depends, of course, on the proper reflective coating. It decreases towards longer and shorter wavelengths, and as rule of thumb, it can be used in a spectral range of about $\lambda_{B1}/2 < \lambda < 2\,\lambda_{B1}$.

Nowadays, *holographic* gratings also are commercially available. They are produced by recording interference fringes on photosensitive material. This procedure results in a groove spacing being absolutely constant and the gratings, therefore, are free of ghosts. The efficiency, however, is lower than that of ruled gratings.

The *linear dispersion* $dx/d\lambda$ in the image plane of the spectrometer determines the separation of two spectral lines. From the grating equation (2) we derive the *angular dispersion* $d\beta/d\lambda$, and by using the equation $x = -f_2\tan\beta$ for the image in the focal plane of the mirror M_2 (the focal length is f_2), we obtain

$$\frac{dx}{d\lambda} = \cancel{\frac{md}{f_2\cos\beta}} \qquad \frac{mf_2}{d\cos^3\beta} \tag{4}$$

Manufacturers very often give the reciprocal linear dispersion $d\lambda/dx$ which measures the number of nanometers that will be found per unit length (or Å/mm).

The *resolving power* R characterizes the minimum separation $\Delta\lambda$ of the central wavelengths of two closely spaced equal intensity lines which are considered to be just resolved. It is defined by

$$R = |\lambda/\Delta\lambda| \tag{5}$$

The theory of diffraction by a grating yields a fundamental limit on the resolving power which, using the Rayleigh criterion for the separation, is expressed by

$$R = mN \tag{6}$$

where N is the total number of grooves on the grating. For a given grating spacing the resolution thus is determined by the width of the grating provided, of course, that the grating indeed is completely and uniformly illuminated. This theoretical maximum of the resolving power is never reached because imperfections of optical components inside the spectrometer and the finite width s_1 of the entrance slit S_1 broaden the diffraction-limited profile of monochromatic radiation in the image plane. The radiant flux entering the spectrometer is proportional to the width of the slit, and a certain width thus is necessary for practical reasons. If the slit width is too small, diffraction at the entrance slit spreads the radiation and a fraction will miss the mirror M_1 reducing the efficiency of the system. Beyond a certain slit width, the profile in the focal plane becomes simply the geometrical image of the slit.

The profile of a spectral line recorded with a spectrograph thus is not the true line profile but broadened by these specific instrumental effects. The profile in the case of extremely monochromatic radiation is called the *apparatus profile* or *instrumental profile* $F(\lambda)$, and it is best obtained experimentally by observing known, very narrow lines. An experimental line profile then is the convolution of the true line profile $f(\lambda)$ and the apparatus profile

$$f_{exp}(\lambda) = \int_{-\infty}^{\infty} f(\mu)\ F(\lambda - \mu)d\mu \qquad (7)$$

Similar considerations apply to a monochromator where the radiant flux through the exit slit of width s_2 is measured. The instrumental profile is obtained by scanning the exit slit across the profile of a narrow line.

For the investigation, a source is usually imaged onto the entrance slit, and the radiance of this image equals the radiance of the source. The radiant flux entering the system thus is determined by the area A_1 of the entrance slit and the solid angle Ω_1 subtended at the entrance slit by the grating. The product $A_1\Omega$ is sometimes named *étendue.* Since the solid angle in the case of a square grating of length D is given by $\Omega_1 = (D/f_1)^2$, the aperture ratio f/D is usually taken as a measure of the light-gathering power of a spectrometer; f/D is called the *f-number.*

The *spectral transmittance* $T(\lambda)$ or *efficiency* of an instrument is determined by the efficiency of the grating and by the reflectivity

$R(\lambda)$ of the mirrors. The selection of proper coatings for optimum reflection poses no problem in this spectral region. For absolute intensity measurements, the transmittance must be known. However, it is usually perferred to determine the absolute sensitivity of the entire system with the detector included.

Overlapping orders, $m\lambda_m$ = const., of a grating spectrometer complicate the identification of spectral lines and, more seriously, may falsify the photoelectrically recorded emission. In many cases, higher orders can simply be suppressed by coloured glass filters, and narrow-band inference filters are used only on those special occasions, where the *stray light* poses a problem in the recording of weak lines or of low continuum radiation. Properly positioned diaphragms may also reduce the level of the stray light somewhat, but the optimum solution are two monochromators in series. If both systems are combined as one unit, we talk of a *double-monochromator*.

The spectrometers allow, to a certain degree, also spatially resolved measurements. The image of the entrance slit is stigmatic, and the different positions along the height of the exit slit thus correspond to different positions in the plasma.

2.3 Types of spectrometers with plane gratings.

Various types of instruments have been designed. Specific tasks and very often a versatile applicability influence the selection of an instrument. The design of Fig. 1 is known as the *Czerny-Turner* mount. It has good resolution, high light-gathering power, a simple scanning mechanism, and the advantage of fixed slits with no deviation in the direction of the exit beam. In the *Ebert-Fastie* mount the mirrors M_1 and M_2 are replaced by a single mirror. Optimum resolution is obtained with curved slits. For other mounts and a discussion of the properties we refer to the literature (1 - 5).

3.
INTERFEROMETER

For high-resolution investigations, which are necessary, for example, when analysing the profiles of emission lines from low-temperature low density plasmas, the *Fabry-Perot* interferometer is probably the most powerful tool. In comparison to any spectrometer, it is the most luminous instrument available for a given resolving power. The basic structure and principles are discussed in almost every textbook on optics, and a most up-to-date description is given in the recent monograph by G. Hernandez(6).

4.
SPECTROMETERS FOR THE VACUUM-ULTRAVIOLET

4.1 Reflectivity

Aluminum is unsurpassed as reflective coating for gratings and mirrors for wavelengths longer than 200 nm. Overcoatings prevent deterioration due to oxidation. Towards shorter wavelengths, however, the reflectance of all materials decreases: at about 100 nm it is generally less than 35% for all materials at normal incidence, and it drops to a few percent at about 300 nm(5). For this reason normal-incidence spectrometers can be used only above 30 nm, and in order to minimize the number of reflections, they generally use a single concave grating which provides dispersion and focusing as well. In principle, it is a spherically concave mirror on which the grooves have been ruled.

For large angles of incidence, on the other hand, total reflection with a reflectance near unity occurs above a critical angle, and this is utilized in a spectrometer design, where the radiation is *grazingly* incident on the grating. If we introduce the grazing angle $\phi = 90^\circ - \alpha$, then ϕ must be selected such that

$$\sin \phi < \frac{\omega}{\omega_p} \tag{8}$$

where ω is the angular frequency of the incident radiation, ω_p the plasma frequency of the free electrons of the metal and α is given in Fig.2. The usable wavelength range follows from this equation (4):

$\lambda/\mathrm{nm} >$ ~~0.55~~ 31 $\sin\phi$ for aluminum oxide

$\lambda/\mathrm{nm} >$ ~~0.27~~ 15 $\sin\phi$ for gold and platinum.

4.2 Concave diffraction gratings

The theory of the concave diffraction grating was developed by H.A. Rowland 100 years ago. He showed that a concave grating of radius R produces a spectrum in focus on a circle of radius R/2 (Rowland circle) which is tangent to the grating, if the entrance slit is on this circle, too (see Fig.3). Vertical focusing occurs outside the circle, and the line image of the entrance slit thus is not stigmatic. This astigmatism of all mountings employing the Rowland circle is the principle drawback and the cause of lower light-gathering power.

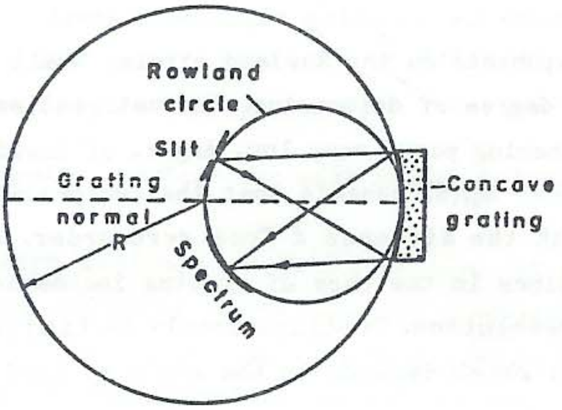

Fig. 3 Rowland mount

The grating equation of the plane grating also holds for the concave grating (Eq.2): The reciprocal dispersion along the Rowland circle is derived as

$$\frac{d\lambda}{dl} = \frac{d\cos\beta}{mR} = \frac{d}{mR}\cos\left(\alpha - \frac{l}{R}\right) \qquad (8)$$

where ℓ is the distance along the Rowland circle measured from zero order.

4.3 Types of spectrometers.

For wavelengths between about 100 nm and 200 nm instruments with plane gratings are also in use. Various normal-incidence mounts employing concave gratings are discussed in the literature(1, 4, 5) and are commercially available(3). When used as spectrograph, the photographic film or plate has to be bent to lie on the Rowland circle. When used as monochromator, at least one of the three components (entrance slit, exit slit or concave grating) has to be moved but in such a way that the Rowland circle condition is obeyed.

Grazing incidence mounting requires highest precision in aligning the three components on the Rowland circle. Small deviations result in a very large degree of defocusing. The astigmatism is considerable and the light gathering power very low. Angles of incidence between 80° and 89° are common. Eq.(8) reveals that the reciprocal dispersion rapidly increases with the distance ℓ from zero order. Large gratings show large aberrations in the case of grazing incidence which, reduces the theoretical resolution. Gratings should be limited, therefore, to an optimum width which depends on the angle of incidence and the wavelength region.

5.

SPECTROMETER FOR THE X-RAY REGION

Eq.(8) indicates that grazing incidence instruments allow, in principle, the recording of spectra down to about 0.5 nm which is considered to be well in the x-ray region. Indeed, the wavelength range up to about 10 nm is called the ultrasoft x-ray region. In general, however, the dispersive elements of spectrometers for x-rays are crystals. The diffraction is governed by Bragg's law

$$m\lambda = 2d \sin\theta \qquad (9)$$

which relates the wavelength λ of the incident x-rays to the glancing angle θ, i.e. the angle between the incident ray and the diffracting plane of the crystal for the n-th order; d is the crystal lattice spacing. If we consider a beam of parallel x-rays incident on a crystal, only those rays will be reflected, whose wavelengths fulfill Bragg`s condition. This leads to a rather straight-forward design, known as Bragg spectrometer (Fig.4). A Soller collimator limits the divergence of the x-rays incident on the crystals. It consists of several parallel plates absorbing any x-rays not propagating parallel to the plates. The Soller collimator may also be placed in front of the detector which reduces the background due to fluorescence in the crystal. A filter is necessary to eliminate the long wavelength radiation. The spectrum is scanned by rotating the crystal and the detector. From the geometry it is obvious that rotation of the crystal by Δθ requires rotation of the detector by 2Δθ. This θ/2θ condition is maintained by special goniometer drives.

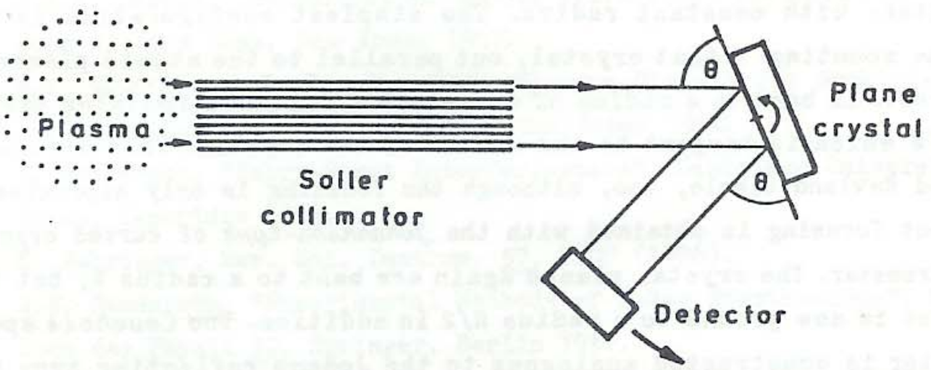

Fig.4 Single crystal spectrometer with Soller collimator

The double crystal monochromater employs two crystals to obtain higher resolution. Two modes of operation are possible: the plus position, where the rays are diffracted in the same sense, and the minus position, where they are deviated in the opposite sense. In general, the diffraction orders used are different for both crystals. The motivation for the selection of such a system may be different, however. An instrument was installed at JET because it offers the possibility of avoiding the direct line of sight from the plasma to the detector. This will be rather critical for operating conditions were high neutron and hard gamma ray fluxes are present(7).

Plane crystal spectrographs are used with point plasmas, which are produced in the vacuum spark discharge (micropinch) or in laser-plasma compression experiments. X-rays of different wavelengths are simply reflected from different positions on the crystal.

Focusing is obtained by bending the crystals to form a cylindrical curvature with constant radius. The simplest configuration is the *Johann* mounting. A flat crystal, cut parallel to the atomic planes of interest, is bent to a radius of curvature R and has a focusing circle of R/2 which is tangent to the centre of the crystal. This circle is called Rowland circle, too, although the focusing is only approximate. Perfect focusing is obtained with the *Johannson-type* of curved crystal spectrometer. The crystal planes again are bent to a radius R, but the surface is now ground to a radius R/2 in addition. The *Couchois* spectrometer is constructed analogous to the Johann reflecting type but used in transmission: the x-ray source is on the convex side of the bent crystal, and the reflecting atomic planes point in radial direction(8).

The performance of all crystal spectrometers certainly depends on the selection of the most suitable crystal and its quality. 2d lattice spacings cover the region from about 0.2 to 14 nm, where the highest values are obtained with multilayer structures. Peak reflectivity, integral reflectivity and resolving power are important parameters(9).

REFERENCES

1. R.A. Sawyer, "Experimental Spectroscopy", Dover Publ., New York, 1963.
2. R.H. Huddlestone and S.L. Leonard, eds., "Plasma Diagnostic Techniques", Academic Press, New York, 1965.
3. W. Lochte-Holtgreven, ed., "Plasma Diagnostics", North-Holland Publ. Co., Amsterdam 1968.
4. J.A.R. Samson, "Techniques of Vaccum Ultraviolet Spectroscopy", John Wiley & Sons, New York, 1967.
5. A.N. Zaidel' and E. Ya. Shreider, "Vacuum Ultraviolet Spektroscopy", Ann Arbor-Humphrey Science Publ., Ann Arbor 1970.
6. G. Hernandez, "Fabry-Perot Interferometers", Cambridge University Press, Cambridge 1986.
7. K. Behringer, Rev. Sci. Instrum. 57, 2000 (1986).
8. A.E. Sandström, "Experimental Methods of X-Ray Spectroscopy", Handbuch der Physik 30, Springer, Berlin 1957.
9. A. Burek, "Space Science Instrumentation", Vol. 2, D. Reidel Publ., Dodrecht, 1976.